THE JOURNAL OF PHYSICAL CHEMISTRY Letters

Letter

pubs.acs.org/JPCL

Structural Properties of Protein−Detergent Complexes from SAXS and MD Simulations

Po-chia Chen* and Jochen S. Hub*

Institute for Microbiology and Genetics, Georg-August-University Göttingen, Justus-von-Liebig weg 11, 37077 Göttingen, Germany

Supporting Information

ABSTRACT: In experimental studies of solubilized membrane proteins, the detergent corona influences the protein behavior and the resulting measurement. Thus, combinations of experimental techniques with atomistic modeling have been used to resolve corona structural parameters and distributions. Here, we used small-angle X-ray scattering (SAXS) data and molecular dynamics simulations to study a model protein−detergent complex (PDC) consisting of aquaporin-0 and dodecyl-β-maltoside molecules (βDDM). The corona morphology of single snapshots was found to be rough, but it is smooth and compacted in 100-ns-scale ensemble averages. Individual snapshots therefore were unable to accurately represent the ensemble information as captured by experimental SAXS. Mimicking of annular lipids by detergent was also observed. SAXS prediction using different published methods was used to identify optimal βDDM numbers. Explicit-solvent methods predicted best agreement using 290-βDDM PDCs, but implicit-solvent methods gave unclear predictions due to overcompensation by free solvation-layer density parameters. Thus, ensemble-based approaches and physically motivated constraints will help to extract structural information from SAXS data.

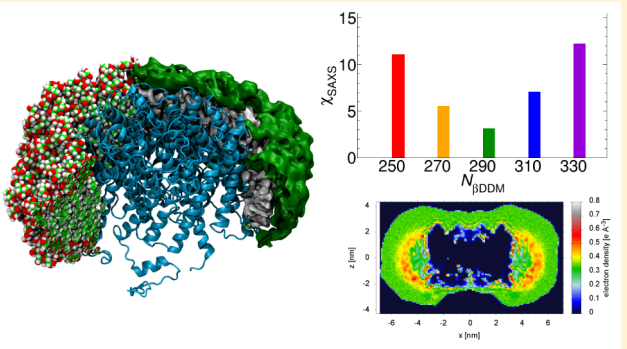

The application of techniques such as small-angle X-ray/neutron scattering (SAXS/SANS),[1−5] mass-spectrometry,[6] solution NMR,[7,8] and Cryo-EM[9] to membrane proteins require their solubilization in membrane-mimicking detergent molecules. The influence of the detergent corona in the resulting protein−detergent complex (PDC) must then be carefully accounted for,[10−12] which has remained challenging due to uncertainties about structural parameters such as detergent aggregation numbers, distribution, and dynamics.

We clarify two significant issues regarding the interpretation of PDC SAXS patterns using atomistic models, by comparing computed SAXS curves based on molecular dynamics simulations (MD) of aquaporin-0 (Aqp0) solubilized in dodecyl-β-maltoside (βDDM) with the experimental SAXS curve measured by Pérez and co-workers[3,13] using novel in-line size-exclusion chromatography to remove pure-detergent micelles.

First, we investigate the extent of conformational sampling required to adequately describe the solution PDC ensemble. The necessity of capturing such thermal fluctuations in SAXS prediction is highlighted by both its known importance for proteins[14−18] and also the widely varying diffusion rates observed in previous PDC and micelle simulations.[19−23] Thus, capturing these PDC shape and size variations in MD may be required to reliably derive conclusions about PDC structural parameters. Second, we test implicit-solvent and explicit-solvent SAXS prediction software[24−29] in the context of mixed protein−detergent environments and examine their ability to extract structural information from the experimental curve. The modeling of buffer and solvation-layer scattering by implicit-solvent approaches require additional fitting parameters that may reduce the amount of usable information. Further, these methods have been primarily tested with pure-protein systems; hence, they may require further refinement for use with PDCs. By addressing these two issues, we highlight approaches and improvements that will best convert measured SAXS patterns into knowledge about the solution PDC ensemble.

Aqp0-βDDM Complex. We first show an example PDC representing the best single-structure fit to experiment according to WAXSiS[29] (Figure 1A,B). PDCs snapshots after ∼100 ns of unbiased MD consistently showed slight asymmetries in shape and were superior in terms of SAXS-agreement than symmetric PDCs at ∼0 ns (Figure S2 in Supporting Information (SI)). The corona surface exhibited significant roughness at all times after equilibration. In each trajectory, 0−2 detergent molecules were found to diffuse into bulk solvent, indicating a low bulk-exchange rate and metastability of the corona.

Predicted SAXS curves based on the PDC snapshot (Figure 1C) show qualitative agreement with experiment. These curves contain two structural properties of interest to us: (1) the number of βDDM comprising the PDC ($N_{\beta DDM}$, aggregation

Received: October 26, 2015
Accepted: December 4, 2015

DOI: 10.1021/acs.jpclett.5b02399
J. Phys. Chem. Lett. 2015, 6, 5116−5121

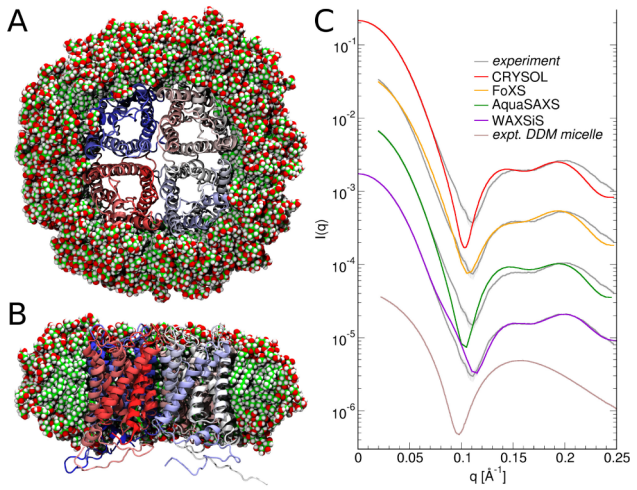

Figure 1. Snapshot of a 290-βDDM PDC and predicted SAXS curves using four SAXS predictors. Top view (A) and side view (B) with detergent removed to reveal lipid tail structure. βDDM are shown as spheres and aquaporin-0 are shown in cartoon form. (C) Predicted SAXS intensities (in colors) scaled to the given experimental curve[13] (gray) and vertically offset for clarity. Software choices are labeled in the legend. A pure βDDM-micelle SAXS curve taken from ref 30 is also shown for comparison.

number) and its corona morphology, most visible from the location and shape of a prominent minimum at q = 0.1 Å^{-1}. The presence of this sharp minimum suggests that the experimental profile contains information on the average size of the PDCs; (2) detergent and Aqp0 organization, observed in the double-peak feature at $q \sim 0.18$ Å^{-1} contrasting a single broad peak in pure micelles (Figure 1C, brown). To test if fluctuations of the protein influence the double-peak structure, SAXS patterns of backbone-restrained PDCs were calculated and compared to results from unrestrained simulations (Figure S3 in SI). We found that backbone-restrained simulations lead to a too-prominent double-peak, suggesting that the strict 4-fold symmetry of the C-terminal tails present in the crystal structure becomes smeared out in solution. On the basis of these qualitative reproductions, the four SAXS prediction software tools shown in Figure 1C were included for further comparisons with MD simulations. (See discussions in SI for excluded software.)

Contribution of Structural Variations to SAXS Patterns. The remaining discrepancies of all computed SAXS patterns in Figure 1C suggests that single structures extracted from MD trajectories do not fully capture the characteristics of the solution ensemble. This may be due to intrinsic structural variations of PDCs, occurring both as conformational fluctuations in individual PDCs as well as variations in detergent aggregation number $N_{\beta DDM}$. We will examine the two sources of variations below.

To test for SAXS contributions from conformational fluctuations, we simulated multiple PDCs trajectories with $N_{\beta DDM}$ ranging between 250 and 330, and then computed ensemble SAXS profiles based on frames between 90−100 ns of MD trajectories, using the explicit-solvent calculations described recently.[18] These ensemble-based SAXS patterns were compared with the above-mentioned SAXS prediction tools, by computing their self-reported χ-agreement to experiment, as shown in Figure 2. SAXS curves related to these χ-values are shown in Figure S4 in SI. A comparison of methodologies shows that WAXSiS and ensemble MD approaches produce a strong discrimination between different $N_{\beta DDM}$ values (Figure 2A−C), with best agreement to experiment at 290 ($\chi_{ensemble}$ = 2.17). Implicit-solvent software tools, in contrast, show (i) little discrimination between different $N_{\beta DDM}$ (Figure 2D−F, black bars) and (ii) higher χ-

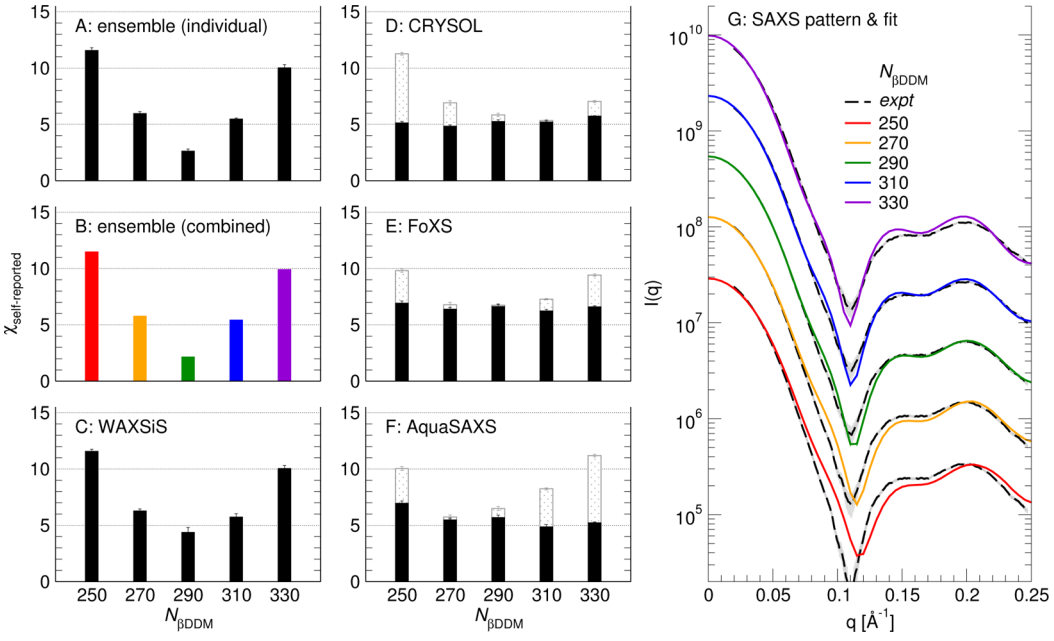

Figure 2. χ-agreement with experimental SAXS of Aqp0-βDDM complexes after 100 ns free simulations, as measured by the software's self-reported χ. Each data point represents average ± SEM of five replica, either with the solvation layer density parameters (C2) fixed ad-hoc (gray, see main text and Figure 3) or optimized to minimize χ (black). SAXS methods are ensemble MD using frames spanning 90−100 ns (A), combination of replica into a single aggregate ensemble (B), WAXSiS (C), CRYSOL (D), FoXS (E), and AquaSAXS (F). SAXS patterns and χ-squared fits corresponding to (B) are shown in (G) in color.

DOI: 10.1021/acs.jpclett.5b02399
J. Phys. Chem. Lett. 2015, 6, 5116−5121

values, despite the fact that they allow the adjustment of more fitting parameters than explicit-solvent approaches (CRYSOL, 3; FoXS, 2; AquaSAXS, 2; WAXSiS, 1; ensemble, 1).

We discuss here the WAXSiS and ensemble results, which can be directly compared because they used the same fitting metric. The general improvement in χ-values of ensemble SAXS over WAXSiS predictions show that the inclusion of detergent and backbone fluctuations lead to improved accuracy. The inclusion of only side chain and hydration-layer fluctuations, as employed by WAXSiS, does not fully capture the solution ensemble. The poor χ values at high or low $N_{\beta DDM}$ further suggests that PDCs possess only small variation in $N_{\beta DDM}$, with the maximum population likely determined, for example, by the amount of detergent required to fully solubilize the membrane protein.

We checked if χ-agreement could be further improved by modeling a population of PDCs with the five $N_{\beta DDM}$ values tested, but we do not find significantly better χ than the single $N_{\beta DDM}$ = 290 result shown above (Figure S5 in SI). Finally, we also tested to include residual pure-DDM micelles as a potential source of contamination. This improves χ from 2.17 to 2.01, but which is likely due to overfitting (see SI discussions). Thus, the experimentally measured PDCs appear to be relatively pure and composed of similar $N_{\beta DDM}$, which permits size information to be directly extracted from SAXS profiles assuming a faithful reproduction of the solution PDC conformations and sufficiently detailed SAXS prediction approaches.

Role of Fitting Parameters in Implicit Solvent Approaches. The lack of χ-discrimination over $N_{\beta DDM}$ shown by all implicit-solvent approaches demands further investigation. In order to model solvent scattering without a water model, these approaches require at least two additional fitting parameters: C1, associated with the buffer contribution in the excluded volume, and C2, the contribution of solvation layer around the solute. Because these are the most likely sources of overfitting, we inspect the C1 and C2-equivalent parameters in CRYSOL, FoXS, and AquaSAXS (Figure 3). A primer on the calculation and fitting procedures adopted by these methods is available in the SI.

The fitted C1 and C2 parameters exhibit a linear dependence upon $N_{\beta DDM}$, although the relative magnitudes differ significantly. A comparison between $N_{\beta DDM}$ = 250 and 330 results shows that an 18% increase in the number of solute atoms in the PDC is associated with a ~1% decrease of C1, and a 3-fold decrease of C2. The small decrease of C1 is expected, because addition of the less electron−dense βDDM will slightly decrease the total buffer contrast. On the other hand, the C2 variations observed span ~40 e nm^{-3}, which is more than the total excess solvation layer density measured in proteins (~33 e nm^{-3}).[31] Given the fact that the solvation environments presented by polar βDDM head groups and exposed protein residues are expected to be very similar, this magnitude appears unphysical. The stark difference between the two parameters suggests that implicit-solvation approaches primarily overfit solvation-layer densities, and not buffer contributions, in order to reconcile a suboptimal $N_{\beta DDM}$ with experiment.

We reinforce the above observations by using AquaSAXS to scan minimum χ achieved, as a function of $N_{\beta DDM}$, C1, and C2 within the software-specified ranges (Figure S6 in SI). AquaSAXS reports a narrow range of acceptable C1 values, within which minimum χ across all tested $N_{\beta DDM}$ are comparable, and C2 variations are expectedly large as seen

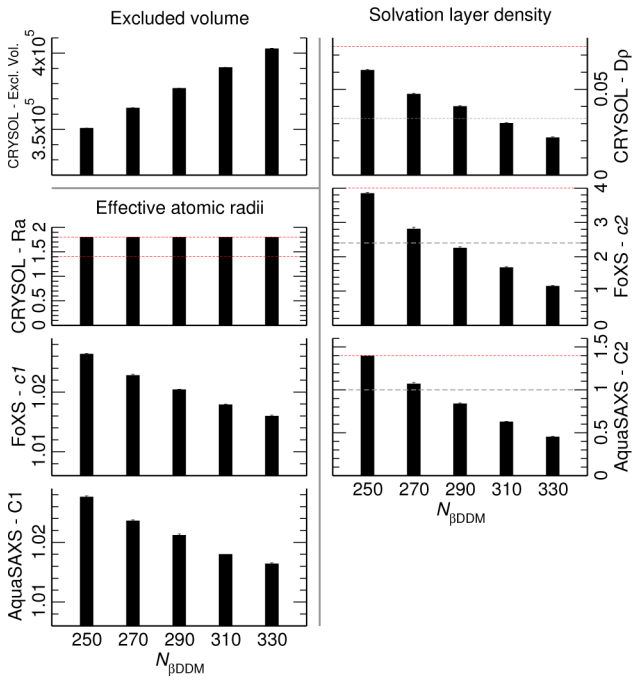

Figure 3. Variations of solvent-related fitting parameters from different SAXS predictors, plotted vs $N_{\beta DDM}$. Each data point represents average and SEM of five replica. Each plot is labeled with the source program and nature of fitting parameter. Left side: parameters controlling buffer scattering (C1-like), including effective atomic radii and excluded volume. Right side: parameters controlling solvation layer scattering (C2-like). Red dotted lines show program fitting limits, and gray-dotted lines show the ad-hoc values used in Figure 2D−F corresponding to ~33 e nm^{-3}.

above (Figure S6A,B in SI, gray area). On the other hand, constraining C2 leads to a restoration of χ-discrimination analogous to explicit-solvent results, because C1 cannot be adjusted to overcompensate for incorrect $N_{\beta DDM}$ (Figure S6C,D in SI). This comparison confirms the solvation-layer modeling and not background subtraction as the main source of overfitting. To test if this finding holds for all implicit-solvent tools, we fixed the solvation-layer density parameters to an ad-hoc value motivated from proteins,[31] which indeed restored limited $N_{\beta DDM}$-discrimination (Figure 2D−F, gray bars). However, without a physical basis to fix the solvation-layer density according to the true underlying βDDM hydration, the correct $N_{\beta DDM}$ cannot be determined. Instead, external information on physically justified C2 values, such as through training-sets or explicit water models, would directly improve the predictive power of implicit-solvent SAXS software.

PDC Shape and Comparisons to Previous Work. As stated above, individual PDCs possess significant surface roughness due to detergent motions (cf. Figure 1 and Figure S7 in SI). However, these variations are smeared in average electron density profiles (Figure S8 in SI), resulting in a smooth micellular surface resembling the toroidal models of the DDM corona.[3,5] A detailed comparison of corona dimensions between ensemble-MD data and one such Memprot model is shown in Figure S9 in SI.

The density profile also shared similar physical dimensions with an independent all-atom model proposed by Pérez et al.[13] (Figure S7 in SI). This Pérez model was generated by constraining MD trajectories using the SAXS-derived physical dimensions and appears slightly more compact than unre-

DOI: 10.1021/acs.jpclett.5b02399
J. Phys. Chem. Lett. 2015, 6, 5116−5121

strained simulations in this work. These pieces of information suggest that implicit-detergent models and single-structure based approaches carried out previously were optimized to the solution ensemble underlying experimental SAXS and do not inform upon the individual PDC fluctuations. This subtle difference may be responsible for a different optimum $N_{\beta DDM}$ identified (270,[13] as opposed to 290 here). Alternatively, the use of implicit hydrogen parameters in Pérez et al. may have affected optimum $N_{\beta DDM}$ estimations. These findings highlight a necessity for caution when interpreting single-structure fits to a solution SAXS pattern.

Detergent Diffusion. A final question pertains to sufficient sampling of MD simulations, because detergent diffusion rates vary widely. The comparison of 90−100 ns and 10−100 ns electron densities (Figure S8 in SI), show that βDDM directly adjacent to Aqp0 diffuse far slower than detergent in the corona "bulk". Although individual lipids are resolvable throughout the corona on the 10 ns time scale, they disappear in the longer average except at sites adjacent to Aqp0. Thus, the simulation ensemble retains little of the starting bias that would otherwise indicate insufficient sampling. This retention of annular detergents echoes the role of annular lipids known from crystallography and membrane simulations.[32] The MD observations here specifically show that Aqp0 also exerts stable lipid sites in a micellular environment.

Summary. In this work, we conducted MD simulations of Aqp0−βDDM complexes at a range of detergent aggregation numbers and examined their agreement with the experimental SAXS profile. The extent of sampling required to replicate experimental distributions, and the ability of a number of SAXS predictors to detect optimal aggregation numbers ($N_{\beta DDM}$) was tested.

We found that explicit-solvent methods retrieve the $N_{\beta DDM}$ information contained in SAXS patterns, but implicit-solvent methods fail without additional physical knowledge. This was due to the latter requiring free fitting parameters for the solvation layer density, which overcompensated for incorrect $N_{\beta DDM}$ and resulted in near-equal χ-values for all structures. Fixing this parameter to an arbitrary value restores χ discrimination, but the optimum $N_{\beta DDM}$ is dependent on both the value adopted and the program used. Thus, a systematic method to estimate the solvation-layer density, perhaps based on exposed chemical moieties, training sets, or explicit-solvent simulations, would improve SAXS information retrieval using implicit-solvent methods.

In terms of PDC shape and size distributions, we further find that a solution ensemble of independent MD trajectories can accurately describe the SAXS curve, whereas individual conformations cannot. This is due to necessary sampling of disordered C-termini and detergent corona. The βDDM corona is morphologically rough on the level of instantaneous snapshots and does not correspond to the smooth densities in the ensemble average. Because the experimental SAXS curve reflects the scattering of the solution ensemble, we recommend adopting ensemble-based approaches in PDC SAXS predictions in order to account for the above-mentioned thermal fluctuations.

The SAXS patterns of the best model distribution yield a χ of ∼2.17, due to remaining deviations near the first minima at q = 0.1 Å^{-1} (Figure 2B, green). We discarded the likelihood that this was due to variations in experimental $N_{\beta DDM}$. Some doubt remains on the sufficiency of our simulation time: although we found metastability over 100 ns time scales, significant detergent rearrangements may occur on longer time scales. Neither can we fully exclude a bias from the applied CHARMM36 force field nor a starting bias from ideal preformed coordinates. These issues deserve further investigation.

While this work demonstrates a superior performance of explicit solvent algorithms in deriving structural parameters of PDCs from SAXS data, we emphasize that in broader contexts both explicit and implicit methods are important in SAXS analysis. Explicit-solvent methods are generally too computationally expensive for applications such as docking and structure determination, where SAXS techniques are commonly utilized. On the other hand, explicit-solvent simulations provide a physical model of the solvation layer that can be used as a guide in implicit-solvent modeling. Thus, a collaborative development between multiple methods will best contribute to SAXS interpretation, as ever more complex systems are addressed.

COMPUTATIONAL METHODS

Force Fields. The CHARMM36 force field,[33,34] as translated into GROMACS,[35,36] was used as a basis of all MD simulations, using the version as of March 2014. Parameters for βDDM are available in CHARMM36. Electrostatic interactions were simulated with particle-mesh Ewald[37] and Lennard-Jones interactions scaled to zero between 10 and 12 Å with a *potential-shift* function.

Micelle formation. Preformed micelles are constructed by aligning Aqp0 along the *Z*-axis and distributing detergent molecules in a spiral around the transmembrane surface. $N_{\beta DDM}$ between 250 and 330 were considered based on previous work.[13] Each molecule was rotated and offset initially to guarantee space between adjacent detergents, then packed via rigid-body motions with a minimum 3.0 Å separation from proteins and ∼1.2 Å from other detergents. Further packing was carried out via 10 ns implicit solvent simulations with protein-backbone restraints, using the generalized Born formalism and OBC method.[38]

MD Simulations. PDCs were solvated with CHARMM-TIP 3p water and 100 mM NaCl in a 163 Å dodecahedron box. A total of 25 replica were simulated (5 at each $N_{\beta DDM}$). Equilibration was conducted via 2500 steps of energy minimization with steepest descent, followed by thermalisation and 20 ns backbone restrained simulations. NPT conditions were maintained through velocity-rescaling (τ_t = 2.5 ps)[39] and Berendsen barostats (τ_p = 5 ps).[40] The time step was set at 4 fs to take advantage of virtual-site construction in GROMACS. Production simulations were unrestrained, and the data between 90−100 ns or 10−100 ns was taken for further calculations, as noted in the Results.

SAXS Calculations. The SAXS predictors used in this study include CRYSOL,[24] FoXS,[28] AquaSAXS,[27] and WAXSiS.[29] AXES[26] and SoftWAXS[25] were tested but have been excluded from comparison due to our inability to fix methodological limitations. Scatter from BIOISIS[41] was also examined but not included. See the SI text for further details and program parameters. For software tools requiring single input conformations, snapshots of PDCs at every 10 ns were used, with the final data at 100 ns presented in the main text. Ensemble SAXS calculations was carried out with an in-house GROMACS distribution.[18,42] Authors of AquaSAXS have kindly provided offline executables. We also emphasize that hydrogens must be explicitly included in FoXS and CRYSOL

DOI: 10.1021/acs.jpclett.5b02399
J. Phys. Chem. Lett. 2015, 6, 5116−5121

calculations to mitigate artifacts in excluded volume (buffer) calculation, likely caused by the lipid tails.

■ ASSOCIATED CONTENT

Supporting Information

The Supporting Information is available free of charge on the ACS Publications website at DOI: 10.1021/acs.jpclett.5b02399.

A primer on included SAXS predictors, additional methodological details on runtime arguments for SAXS predictors, convergence as measured by SAXS, SAXS curves of all predictions, analysis of AquaSAXS fitting parameters, structural characteristics of the simulated micelles, and Figures S1−S9. (PDF)

■ AUTHOR INFORMATION

Corresponding Authors

*E-mail: po-chia.chen@univ-lyon1.fr; Web: https://www.researchgate.net/profile/Po_Chia_Chen.
*E-mail: jhub@gwdg.de.

Present Address

(P.-c.C.) Institut des Sciences Analytiques, UMR 5280, CNRS, Université de Lyon, 5 Rue de la Doua, 69100 Villeurbanne, France.

Notes

The authors declare no competing financial interest.

■ ACKNOWLEDGMENTS

We thank the authors of AquaSAXS for providing an offline version of their SAXS prediction software, and Javier Pérez for experimental SAXS data as well as the coordinates of their best-fit Aqp0-βDDM model. We also thank Frédéric Poitevin (AquaSAXS), Alex Grishaev (AXES), and Javier Pérez for insightful discussions. This study was supported by the Deutsche Forschungsgemeinschaft (HU 1971/1-1).

■ REFERENCES

(1) Rambo, R. P.; Tainer, J. A. Super-Resolution in Solution X-Ray Scattering and Its Applications to Structural Systems Biology. *Annu. Rev. Biophys.* **2013**, *42*, 415−441. PMID: 23495971.

(2) Cardoso, M. B.; Smolensky, D.; Heller, W. T.; O'Neill, H. Insight into the Structure of Light-Harvesting Complex II and Its Stabilization in Detergent Solution. *J. Phys. Chem. B* **2009**, *113*, 16377−16383.

(3) Berthaud, A.; Manzi, J.; Pérez, J.; Mangenot, S. Modeling Detergent Organization around Aquaporin-0 Using Small-Angle X-ray Scattering. *J. Am. Chem. Soc.* **2012**, *134*, 10080−10088.

(4) Gabel, F.; Lensink, M. F.; Clantin, B.; Jacob-Dubuisson, F.; Villeret, V.; Ebel, C. Probing the Conformation of FhaC with Small-Angle Neutron Scattering and Molecular Modeling. *Biophys. J.* **2014**, *107*, 185−196.

(5) Pérez, J.; Koutsioubas, A. *Memprot*: A Program to Model the Detergent Corona Around a Membrane Protein Based on SEC- SAXS Data. *Acta Crystallogr., Sect. D: Biol. Crystallogr.* **2015**, *71*, 86−93.

(6) Rouse, S. L.; Marcoux, J.; Robinson, C. V.; Sansom, M. S. Dodecyl Maltoside Protects Membrane Proteins In Vacuo. *Biophys. J.* **2013**, *105*, 648−656. PMID: 23931313. PMCID: PMC3736684.

(7) Fernández, C.; Hilty, C.; Wider, G.; Wüthrich, K. Lipid−Protein Interactions in DHPC Micelles Containing the Integral Membrane Protein OmpX Investigated by NMR Spectroscopy. *Proc. Natl. Acad. Sci. U. S. A.* **2002**, *99*, 13533−13537. PMID: 12370417.

(8) Columbus, L.; Lipfert, J.; Jambunathan, K.; Fox, D. A.; Sim, A. Y. L.; Doniach, S.; Lesley, S. A. Mixing and Matching Detergents for Membrane Protein NMR Structure Determination. *J. Am. Chem. Soc.* **2009**, *131*, 7320−7326.

(9) Vahedi-Faridi, A.; Jastrzebska, B.; Palczewski, K.; Engel, A. 3D imaging and quantitative analysis of small solubilized membrane proteins and their complexes by transmission electron microscopy. *Microscopy* **2013**, *62*, 95−107.

(10) Marsh, D. Protein Modulation of Lipids, and Vice-Versa, in Membranes. *Biochim. Biophys. Acta, Biomembr.* **2008**, *1778*, 1545−1575.

(11) Cross, T. A.; Sharma, M.; Yi, M.; Zhou, H.-X. Influence of Solubilizing Environments on Membrane Protein Structures. *Trends Biochem. Sci.* **2011**, *36*, 117−125.

(12) Oliver, R. C.; Lipfert, J.; Fox, D. A.; Lo, R. H.; Doniach, S.; Columbus, L. Dependence of Micelle Size and Shape on Detergent Alkyl Chain Length and Head Group. *PLoS One* **2013**, *8*, e62488.

(13) Koutsioubas, A.; Berthaud, A.; Mangenot, S.; Pérez, J. Ab Initio and All-Atom Modeling of Detergent Organization around Aquaporin-0 Based on SAXS Data. *J. Phys. Chem. B* **2013**, *117*, 13588−13594.

(14) Bernadò, P.; Mylonas, E.; Petoukhov, M. V.; Blackledge, M.; Svergun, D. I. Structural Characterization of Flexible Proteins Using Small-Angle X-ray Scattering. *J. Am. Chem. Soc.* **2007**, *129*, 5656−5664.

(15) Park, S.; Bardhan, J. P.; Roux, B. t.; Makowski, L. Simulated X-Ray Scattering of Protein Solutions Using Explicit-Solvent Models. *J. Chem. Phys.* **2009**, *130*, 134114.

(16) Köfinger, J.; Hummer, G. Atomic-Resolution Structural Information from Scattering Experiments on Macromolecules in Solution. *Phys. Rev. E* **2013**, *87*, 052712.

(17) Moore, P. B. The Effects of Thermal Disorder on the Solution-Scattering Profiles of Macromolecules. *Biophys. J.* **2014**, *106*, 1489−1496.

(18) Chen, P.-c.; Hub, J. S. Validating Solution Ensembles from Molecular Dynamics Simulation by Wide-Angle X-ray Scattering Data. *Biophys. J.* **2014**, *107*, 435−447.

(19) Braun, R.; Engelman, D. M.; Schulten, K. Molecular Dynamics Simulations of Micelle Formation around Dimeric Glycophorin A Transmembrane Helices. *Biophys. J.* **2004**, *87*, 754−763.

(20) Bond, P. J.; Cuthbertson, J. M.; Deol, S. S.; Sansom, M. S. P. MD Simulations of Spontaneous Membrane Protein/Detergent Micelle Formation. *J. Am. Chem. Soc.* **2004**, *126*, 15948−15949.

(21) Khao, J.; Arce-Lopera, J.; Sturgis, J. N.; Duneau, J.-P. Structure of a Protein- Detergent Complex: The Balance Between Detergent Cohesion and Binding. *Eur. Biophys. J.* **2011**, *40*, 1143−1155.

(22) Khelashvili, G.; LeVine, M. V.; Shi, L.; Quick, M.; Javitch, J. A.; Weinstein, H. The Membrane Protein LeuT in Micellar Systems: Aggregation Dynamics and Detergent Binding to the S2 Site. *J. Am. Chem. Soc.* **2013**, *135*, 14266−14275.

(23) Rouse, S. L.; Sansom, M. S. P. Interactions of Lipids and Detergents with a Viral Ion Channel Protein: Molecular Dynamics Simulation Studies. *J. Phys. Chem. B* **2015**, *119*, 764−772.

(24) Svergun, D.; Barberato, C.; Koch, M. H. J. CRYSOL − a Program to Evaluate X-ray Solution Scattering of Biological Macromolecules from Atomic Coordinates. *J. Appl. Crystallogr.* **1995**, *28*, 768−773.

(25) Bardhan, J.; Park, S.; Makowski, L. SoftWAXS: A Computational Tool for Modeling Wide-Angle X-Ray Solution Scattering from Biomolecules. *J. Appl. Crystallogr.* **2009**, *42*, 932−943. PMID: 21339902. PMCID: PMC3041499.

(26) Grishaev, A.; Guo, L.; Irving, T.; Bax, A. Improved Fitting of Solution X-ray Scattering Data to Macromolecular Structures and Structural Ensembles by Explicit Water Modeling. *J. Am. Chem. Soc.* **2010**, *132*, 15484−15486.

(27) Poitevin, F.; Orland, H.; Doniach, S.; Koehl, P.; Delarue, M. AquaSAXS: A Web Server for Computation and Fitting of SAXS Profiles with Non-Uniformally Hydrated Atomic Models. *Nucleic Acids Res.* **2011**, *39*, W184−W189. PMID: 21665925.

(28) Schneidman-Duhovny, D.; Hammel, M.; Tainer, J. A.; Sali, A. Accurate SAXS Profile Computation and its Assessment by Contrast Variation Experiments. *Biophys. J.* **2013**, *105*, 962−974.

(29) Knight, C. J.; Hub, J. S. WAXSiS: A Web Server for the Calculation of SAXS/WAXS Curves Based on Explicit-Solvent

DOI: 10.1021/acs.jpclett.5b02399
J. Phys. Chem. Lett. 2015, 6, 5116−5121

Molecular Dynamics. *Nucleic Acids Res.* **2015**, *43*, gkv309. PMID: 25855813.
(30) Lipfert, J.; Columbus, L.; Chu, V. B.; Lesley, S. A.; Doniach, S. Size and Shape of Detergent Micelles Determined by Small-Angle X-ray Scattering. *J. Phys. Chem. B* **2007**, *111*, 12427−12438.
(31) Svergun, D. I.; Richard, S.; Koch, M. H. J.; Sayers, Z.; Kuprin, S.; Zaccai, G. Protein hydration in solution: Experimental observation by x-ray and neutron scattering. *Proc. Natl. Acad. Sci. U. S. A.* **1998**, *95*, 2267−2272. PMID: 9482874.
(32) Aponte-Santamaría, C.; Briones, R.; Schenk, A. D.; Walz, T.; Groot, B. L. d. Molecular Driving Forces Defining Lipid Positions Around Aquaporin-0. *Proc. Natl. Acad. Sci. U. S. A.* **2012**, *109*, 9887−9892. PMID: 22679286.
(33) Brooks, B. R.; Brooks, C. L.; Mackerell, A. D.; Nilsson, L.; Petrella, R. J.; Roux, B.; Won, Y.; Archontis, G.; Bartels, C.; Boresch, S.; et al. CHARMM: The Biomolecular Simulation Program. *J. Comput. Chem.* **2009**, *30*, 1545−1614.
(34) Best, R. B.; Zhu, X.; Shim, J.; Lopes, P. E. M.; Mittal, J.; Feig, M.; MacKerell, A. D. Optimization of the Additive CHARMM All-Atom Protein Force Field Targeting Improved Sampling of the Backbone ϕ, ψ and Side-Chain χ1 and χ2 Dihedral Angles. *J. Chem. Theory Comput.* **2012**, *8*, 3257−3273.
(35) Hess, B.; Kutzner, C.; van der Spoel, D.; Lindahl, E. GROMACS 4: Algorithms for Highly Efficient, Load-Balanced, and Scalable Molecular Simulation. *J. Chem. Theory Comput.* **2008**, *4*, 435−447.
(36) Bjelkmar, P.; Larsson, P.; Cuendet, M. A.; Hess, B.; Lindahl, E. Implementation of the CHARMM Force Field in GROMACS: Analysis of Protein Stability Effects from Correction Maps, Virtual Interaction Sites, and Water Models. *J. Chem. Theory Comput.* **2010**, *6*, 459−466.
(37) Essmann, U.; Perera, L.; Berkowitz, M. L.; Darden, T.; Lee, H.; Pedersen, L. G. A Smooth Particle Mesh Ewald Method. *J. Chem. Phys.* **1995**, *103*, 8577−8593.
(38) Onufriev, A.; Bashford, D.; Case, D. A. Exploring Protein Native States and Large-Scale Conformational Changes with a Modified Generalized Born Model. *Proteins: Struct., Funct., Genet.* **2004**, *55*, 383−394.
(39) Bussi, G.; Donadio, D.; Parrinello, M. Canonical Sampling Through Velocity Rescaling. *J. Chem. Phys.* **2007**, *126*, 014101.
(40) Berendsen, H. J. C.; Postma, J. P. M.; Gunsteren, W. F. v.; DiNola, A.; Haak, J. R. Molecular Dynamics with Coupling to an External Bath. *J. Chem. Phys.* **1984**, *81*, 3684−3690.
(41) Classen, S.; Hura, G. L.; Holton, J. M.; Rambo, R. P.; Rodic, I.; McGuire, P. J.; Dyer, K.; Hammel, M.; Meigs, G.; Frankel, K. A.; et al. Implementation and performance of SIBYLS: a dual endstation small-angle X-ray scattering and macromolecular crystallography beamline at the Advanced Light Source. *J. Appl. Crystallogr.* **2013**, *46*, 1−13.
(42) Chen, P.-c.; Hub, J. S. Interpretation of Solution X-Ray Scattering by Explicit-Solvent Molecular Dynamics. *Biophys. J.* **2015**, *108*, 2573−2584.

DOI: 10.1021/acs.jpclett.5b02399
J. Phys. Chem. Lett. 2015, 6, 5116−5121